Brass-texture induced grain structure evolution in room temperature rolled ODS copper

S. M. S. Aghamiri[1,*], N. Oono[1], S. Ukai[1], R. Kasada[2], H. Noto[3], Y. Hishinuma[3], T. Muroga[3]

[1]*Graduate School of Engineering, Hokkaido University, Sappor 060-8628, Japan*

[2] *Institute of Materials Research, Tohoku University, sendai 980-8577, Japan*

[3]*National Institute of Fusion Science, Gifu 509-5202, Japan*

Abstract

Currently, advanced ODS copper alloy is under study as a potential fusion material providing good mechanical properties. In this work, in order to develop a high performance ODS copper containing 0.5wt% Y_2O_3 oxide particles, the effect of room temperature rolling and subsequent annealing on the grain structure evolution, texture development and tensile properties are studied using EBSD, TEM and tensile tests. Microstructure evolution studies show the grain structure coarsens by enhancing the Brass texture during increase of rolling reduction and a unique single crystal-like brass-texture deformed structure is achieved after 80% rolling reduction. We found the deformation mechanism of partial slip by $\frac{a}{6}\langle 211\rangle$ dislocations facilitated by the pinning of $\frac{a}{2}\langle 101\rangle$ perfect dislocations through fine oxide particles is responsible for formation of Brass texture during room temperature rolling. Furthermore, the recrystallization of ODS copper retards to high temperature of ~700°C and shows a fine-grained microstructure with different orientations of Goss, Brass, S and Copper. Evaluation of microstructure-mechanical properties of the recrystallized samples expresses that the bimodal grain size distribution at 800°C for 30 min offers a good tensile strength-ductility (UTS: 491 MPa, el_t: 19%) at ambient temperature.

Keywords: ODS copper; Grain structure; Brass texture; Tensile properties; Rolling and Recrystallization

* Corresponding author. Hokkaido University, Sappor 060-8628, Japan.

Email Address: sms.aghamiri@gmail.com

1. Introduction

Advanced oxide dispersion strengthened (ODS) materials are attractive category of metallic alloys especially for the neutron irradiation environments due to the good mechanical properties and radiation resistance by suppression of irradiation defects using fine dispersion of Y-based oxide particles in the microstructure. During the recent decades, different types of ODS steels have been developed successfully for application in the nuclear fission reactors [1]. Recent attention to fusion energy as infinite source of energy has been a strong motivation for a broader area of structural materials research like new ODS copper alloys for high heat flux applications in some fusion reactor components such as divertor [2, 3]. In this way, the control of microstructure offering good mechanical properties at low to intermediate temperature is of paramount importance.

It is well known that plastic deformation by cold rolling and subsequent recrystallization is an effective way of microstructure control to improve mechanical properties. In recent years, this processing especially at cryogenic temperatures attracted a considerable attention [4, 5]. During such processing of metallic alloys, the evolution of grain size and preferred texture are two important microstructural parameters of materials which strongly affect different mechanical/physical properties such as tensile strength, strain hardening, ductility and also thermal conductivity [6-8]. It has been well documented that by plastic deformation of metallic alloys at low temperature, the density of defects rises up, i.e. dislocations pile-up and increase

in grain boundaries through change in grain shape results in deformation induced grain refinement [9, 10]. In other side, literature review shows that the effect of primary grain size on the evolution of texture is considerable [11-14]. In a new paper, Gu et al. [6] achieved a brass-type texture in the ultrafine grained copper, while a copper-type texture was obtained in the coarse-grained copper after the same rolling condition and concluded that the deformation texture in severe rolled copper is strongly grain size dependent.

It has been observed generally that fcc materials develop two different types of rolling texture depending on material parameters especially stacking fault energy (SFE): α-fiber or brass-type texture in low SFE materials and β-fiber or copper-type texture in medium to high SFE materials. The α-fiber is described by a combination of the brass orientation ($\{110\}\langle 2\bar{1}1\rangle$) and the Goss orientation ($\{110\}\langle 100\rangle$) while the β-fiber is obtained by the main orientations of copper ($\{112\}\langle 111\rangle$) and S ($\{123\}\langle 634\rangle$). It is widely accepted that copper type texture is developed by homogenous deformation of polycrystal with straight-forward $\{111\}\langle 110\rangle$ slip based on the Taylor model, but still the underlying mechanisms related to the formation of brass type texture is a controversial subject. Leffers and Ray [15] in a recent review paper explained the current understanding on main parameters affecting on the brass-type texture development. It is believed that deformation twinning has a decisive effect on development of the brass-type texture via overshooting/latent hardening introduced by the closely spaced twin lamellae. In addition, shear bands have been observed to provide a predominant contribution during the late

stages of the development of the brass-type texture [5,16]. Recently, some researchers have investigated the effect of deformation mechanism on development of Brass-type texture [17, 18]. Gu et al. [18] discussed the deformation mechanism of brass-type texture in rolling of ultrafine-grained copper associated with the activation of partial $\{111\}\langle 11\bar{2}\rangle$ slip in addition to usual $\{111\}\langle 110\rangle$ slip and with a reduced quantity of geometrically necessary dislocations using the viscoplastic self-consistent polycrystal model.

The distribution of second phase particles in the metallic matrix has been observed to be an effective factor on the deformation microstructure and texture. Hansen and Leffer [19] have reviewed the role of small and large particles in fcc materials during deformation and pointed out that presence of oxide particles leads to higher dislocation density and smaller subgrain size in a given strain. For small volume fractions of particles, the texture strengthening has been reported in some studies. Even though in recent years many researches have tried to understand the microstructure evolution of pure copper during rolling deformation, the information on the evolution of microstructure and texture of oxide dispersion strengthened copper is quite low. The objective of this work is to specify the crystallographic texture of ODS copper and its effect on the grain structure evolution during rolling deformation at room temperature and subsequent recrystallization annealing and assess underlying deformation mechanism and related tensile properties by experimental evaluations.

2. Experimental

In this study, ODS copper material with a nominal composition of Cu-0.5wt% Y_2O_3 was prepared. A high purity (99.9%) copper powder with the mean particle size of 50 μm and Y_2O_3 nanopowder with the mean particle size of 50 nm were used as raw materials. The powder mixture was mechanically alloyed (MA) by using Fritch-P6 planetary ball mill with optimum amount of 1wt% stearic acid as process control agent in Ar gas atmosphere. The ball milling was performed for 48 hours with ball to powder ratio of 10:1 and rotation speed of 470 rpm. The chemical composition of MA powder has been shown elsewhere [20]. Then, the MA powder was consolidated by spark plasma sintering (SPS) in a graphite die at 900ºC/45min under a load of 800 kg and a vacuum of 10 Pa. After the consolidation, a sintered ODS copper with a cylindrical shape of ~ 15 mm (diameter) × 10 mm (height) was obtained and a sample with a thickness of 3 mm was cut from the center part normal to the radial direction for subsequent rolling and microstructural analysis.

Cold rolling process was performed on the sintered ODS copper sample at room temperature with a total thickness reduction of 80% and a low thickness reduction of 0.01 mm per pass using a two-rolling mill with the roll diameter of 160 mm. For comparison, a sintered pure copper sample without Y_2O_3 oxide particles was cold rolled with the same conditions. The Evolution of microstructure and rolling texture during deformation was evaluated by stopping the cold rolling process at different thickness reductions of 20%, 40%, 60% and 80%. Then the annealing was done on 80% cold rolled samples in temperature range of 100-900ºC

for 30 min to evaluate the recrystallization temperature.

X-ray diffraction was conducted by means of $Cu - K_\alpha$ radiation with a Philips X´Pert PRO to measure the dislocation density according to Ref. [20]. The analysis was performed on the surface of polished 80% rolled plates with an acceleration voltage of 40 kV and the current of 40 mA in the 2θ range of 20º-100º with a step size of 0.02º. The microstructure of specimens was observed by electron backscatter diffraction (EBSD) equipment attached to a field emission scanning electron microscope (JEOL JSM-6500F) operating at 15 kV. The observations were made on the rolling plane containing rolling direction (RD) and transverse direction (TD) in the mid-thickness section of the samples with a step size depending on the grain size as low as 20 nm. Sample preparation for EBSD was done by grinding with SiC paper up to 2000 grit and then polishing with 1 μm diamond paste and final polishing with Struers colloidal silica suspension. To attain EBSD data, TSL-OIM software was used for different analyses of inverse pole figure (IPF) maps, image quality (IQ) map, orientation distribution functions (ODF) and grain size measurements. To improve the reliability of the EBSD data, small grains comprising three or fewer pixels were automatically removed from the maps using the grain-dilation option in the software. Furthermore, a lower limit boundary-misorientation cutoff of 2° was used and a 15° criterion was employed to differentiate low-angle boundaries (LABs) and high-angle boundaries (HABs). Grain size was quantified by the determination of the area of each grain and the calculation of its circle-equivalent diameter. To evaluate the

texture, ODF related to three different sections in $\varphi_2 = 0°, 45°, 65°$ were studied based on the typical orientations of fcc structure.

A JEOL JEM-2010 transmission electron microscopy was used with a voltage of 200 kV to study the microstructures of rolled samples in high magnification. To study the dislocations in the microstructures, the sample tilted in four different g-vectors near to [011] zone axis. Furthermore, a FEI-Titan scanning transmission electron microscope (300 kV) was used to analyze fine oxide particles. The thin foil for TEM observation was prepared by focused ion beam (FIB) (JEOL JIB-4600F) and the thinning was accomplished up to the thickness of ~100 nm. For evaluation of oxide particle distribution, the average particle size and the number density of oxide particles was derived in thin foil based on TEM images using the convergent-beam technique [20,21]. The volume fraction of twin bundles was estimated based on different TEM images taken in different areas. Considering the same thickness in the TEM images, the volume fraction of twin bundles was evaluated.

To specify the recrystallization temperature, Vickers microhardness data of the rolled and annealed samples were obtained by a HMV-Micro Hardness Tester-SHIMADZU, under a load of 980 mN and dwell time of 30 s with 5 times measurements. The average Vickers microhardness values were reported, and the maximum and minimum values were shown as error bar. In order to evaluate mechanical properties, uniaxial tensile tests were performed parallel to the rolling direction at ambient temperature under a strain rate of $1.0 \times 10^{-3}\ s^{-1}$

using Shimadzu, SSL-1KN tensile machine. For each condition, two miniaturized size specimens were prepared with a gauge dimension of 5 mm in length, 1.2 mm in width and 0.5 mm in thickness using an electro-discharge processing machine.

3. Results

3.1. Microstructure characterization after sintering and rolling of 80% reduction

Fig. 1 shows the EBSD results of sintered ODS copper by SPS at 900ºC/45 min. IPF map of sintered ODS copper (Fig. 1(a)) exhibits mainly submicron sized grains (~80% area fraction) in combination with some larger micron sized grains were formed in the microstructure. The misorientation distribution of grain boundaries (Fig. 1(b)) shows that about 40% area fraction of boundaries are LABs of <15º and 60% are HABs with a peak around 60º related to twin boundaries. The related ODF (Fig. 1(c)) at $\varphi_2 = 0°$ indicates that a main texture of α-fiber with the maximum intensity of 2.7 was developed in sintered microstructure from Goss ($\{011\}\langle 100\rangle$) to around Brass orientation ($\{011\}\langle 2\bar{1}1\rangle$) together with weaker texture near to β-fiber (including copper$\{112\}\langle 111\rangle$ and S$\{123\}\langle 634\rangle$) and Y orientation ($\{111\}\langle 2\bar{1}1\rangle$) . Formation of this texture in the sintered ODS copper after SPS is in contrast to random texture reported for sintered pure copper [22]. However, after rolling with 80%reduction, the IPF map of rolling plane in Fig. 2(a) reveals the formation of an unexpected microstructure of large green grain with some fine grains distributed inside the matrix. The related image quality (IQ) map in Fig. 2(b) expresses low IQ values attributed to high stored energy in the large green

grain. The supplementary results indicate formation of a large grain in three dimensions of rolling, transverse and normal directions. The texture determined by the ODF in $\varphi_2 = 0°$ (Fig. 2(c)) demonstrates concentration of strong Brass orientation ($\{011\}\langle 2\bar{1}1\rangle$) with a high maximum intensity of 143 times than random which was confirmed by strong peak of $\{022\}$ plane in X-ray measurement (not shown here). Fig. 2 (d) shows the grain boundary map of the same frame of the IPF map in Fig. 2 (a) as the HABs are shown in black line and the LABs of 2-5° and 5-15° are shown with red and green lines, respectively. It clearly expresses that the large green grain is covered mainly by many fine subgrains with approximate size of 100 nm via arrangement of LABs of <5º in the curved shape in addition to some grains delineated by HABs with a size in the range of 100 nm-5 μm. The misorientation distribution of grain boundaries in Fig. 2 (e) illustrates that 74% area fraction is belonged to the LABs of <5º which increased considerably after cold rolling. In comparison, in the work by Gu et al. [18], sub-micrometer grains with a brass-type texture including 11.2% copper, 39% S and 34% Brass orientations was accomplished after high strain rolling of ultrafine-grained copper.

Fig. 3(a) shows the bright-field (BF) TEM image of ODS copper sintered around 900ºC before cold rolling with 80% reduction. It can be seen many fine submicron sized grains are distributed in the microstructure of sintered ODS copper as confirmed by inset diffraction pattern with a relatively high dislocation density remained in the microstructure after the sintering. Another important microstructural property illustrated by diffraction pattern and BF-

STEM image in Fig. 3(b) is fine distribution of Y_2O_3 oxide particles in the microstructure of the sintered ODS copper. Based on this figure, fringe patterns appear in the interface of oxide particles with copper matrix, suggesting semicoherent interface of oxide particles. The fringe contrast has been discussed for oxide particles in literature to be formed by the misfit dislocations [20, 23]. Number density of oxide particles was estimated in the order of 1.62×10^{22} m^{-3} with an average diameter of ~10nm. This high distribution of fine oxide particles has a strong effect on capturing the irradiation defects at the interface of oxides-matrix and contributing to irradiation resistance [1]. TEM observations from the microstructure of 80% rolled ODS copper in Fig. 3(c) suggests the fine nanosized subgrains or grains as shown by arrows with a size of ~100 nm have been distributed in the matrix as confirmed by the inset diffraction pattern from $[211]$ zone axis. Some nanoscale deformation twin bundles [24] with lenticular shape can be seen in Fig. 3(d) spreading in various high strain areas which was estimated to be about 6% of area fraction. Furthermore, a high dislocation density was accumulated in the whole microstructure which was calculated to be 1.00×10^{15} m^{-2}, one order of magnitude higher in compared to the value of 1.82×10^{14} m^{-2} for the 80% reduction rolled pure copper without oxide particles. The TEM results are consistent with EBSD results in Fig. 2, showing the formation of many fine subgrains inside the matrix of large Brass-texture grain by arrangement of dislocation boundaries discussed previously for different cold rolled fcc metals [25-27], and indicating a unique deformed structure was developed in heavily cold

rolled ODS copper.

3.2. Evolution of grain structure and texture during cold rolling

To evaluate the evolution of grain structure and crystallographic texture during cold rolling of ODS copper, the rolling plane microstructure was analyzed by EBSD in different thickness reductions of 20%, 40%, 60% and 80%, respectively (Fig. 4). Based on the IPF maps, the grains after 20% reduction are in fine submicron size with the distribution of some green grains of $\{110\}$ rolling plane (Fig. 4a), then by increasing the reduction to 40% and 60%, the density of green grains increase with simultaneous growth of the grain size especially after 60% to micron size (Fig. 4b, c). Surprisingly, after 80% reduction (Fig. 4d), one green grain overspread in the whole microstructure and a single crystal-like structure formed in the final cold rolled ODS copper material. It should be noted that the analysis was done in the lowest feasible magnification with a 1 mm scale to show the magnitude of the single grain. As observed in the ODF (Fig. 4(e-h)), the crystallographic texture of Brass orientation ($(110)[2\bar{1}1]$) is dominant in all reductions. While in deformation textures up to 60% reduction, some scattering of texture around Brass orientation is also available related to the grains with other orientations, the texture of 80% rolled sample was converged completely around Brass orientation with much higher intensity. Formation of such a microstructure is in contrast to the usual cold rolled microstructures in pure copper [28] and demonstrates an extraordinary deformed structure based on our literature survey.

Fig. 5 depicts the change in grain size, grain boundary length fraction and Brass-texture intensity (defined as the ratio of weight at Brass orientation relative to its weight in a random texture) versus different rolling reductions based on the EBSD results of Fig. 4. As shown in Fig. 5(a), the primary sub-micron sized grains, by starting cold rolling to 20% reduction remains in ultrafine grain size of 0.25±0.21 μm, then by increasing rolling reduction the grain size start to grow slowly and reaches to 0.27±0.21 μm and 0.31±0.31 μm after 40% and 60% reductions, respectively. By progress of rolling to more heavy deformation, the trend of grain growth accelerates and after final 80% reduction, an interestingly single grain with a several millimeter-sized grain forms in the microstructure. Furthermore, analysis of grain boundary length fractions of LABs (2-15°) and HABs (>15°) taken from the equivalent area in Fig. 5(b) determines a consistent result with a stable ratio of about 40% LABs and 60%HABs up to 60% reductions and then the fraction of the LABs increase significantly to ~83% with remaining 17% LABs as seen in Fig. 2(d). The progress of the intensity of Brass texture during rolling reductions up to 80% can be observed in Fig. 5(c). This curve shows the intensity of Brass texture is incrementing slowly from 2.7 times in primary sample to 14.5 times in 60% reductions, then by increase of rolling to 80% reduction, the intensity rose considerably up to 143 times. In comparison to the change of grain size, this curve shows the same evolution during rolling and expresses the dependency of grain growth to texture intensity during heavy deformation by cold rolling.

3.3. Evolution of grain structure and texture during annealing and related mechanical properties

To study subsequent recrystallized microstructures, the Vickers microhardness ($HV_{0.1}$) of cold rolled ODS copper samples were analyzed after annealing at different temperatures of 100-900ºC for 30 min (Fig. 6). In the figure, there is a little drop from microhardness of 80% rolled condition ($171\pm3HV_{0.1}$) by annealing at low temperatures up to around 600ºC probably due to thermally activated recovery processes. However, at temperature range of ~700-800 ºC, the microhardness showed a high drop to the value of $123\pm1HV_{0.1}$ and $106\pm5HV_{0.1}$ at 700ºC and 800 ºC, respectively, suggesting the occurrence of static recrystallization phenomena [29].

Fig. 7 (a,b) shows the EBSD results of recrystallized ODS copper at 700 ºC and 800 ºC for 30 min after 80% reduction rolling. The microstructure of recrystallized ODS copper at 700ºC/30 min in the IPF map (Fig. 7a) exhibits formation of fine new grains in the wide range of submicron to micron sized grains with average grain size of ~0.46μm. The related ODF at $\varphi_2 = 0°, 45°, 65°$ indicate that the new grains have different orientations in α-fiber including Goss ($\{011\}\langle100\rangle$) and Brass ($\{011\}\langle2\bar{1}1\rangle$) orientations and also β-fiber including S ($\{123\}\langle634\rangle$) and copper ($\{112\}\langle111\rangle$) orientations. By increasing recrystallization to 800ºC/30 min (Fig. 7b), a larger average grain size of 0.53 μm formed in the sample and some abnormal grain growth can be observed in the micrometer sized grains in combination to the ultrafine grains in the IPF map, however the texture still remained in the α-fiber and β-fiber

including the main orientations of Goss, Brass, S and copper with the higher texture intensity of 12.4 in compared to recrystallization at 700ºC.

Fig. 8 shows the engineering tensile stress-strain curves of 80% reduction rolled ODS copper and subsequent recrystallized ODS copper at 700°C and 800°C for 30 min, evaluated at ambient temperature. The related values of mechanical properties including yield strength ($\sigma_{0.2}$), ultimate strength (σ_u), uniform elongation (el_u) and total elongation (el_t) can be seen in Table 1. As observed clearly in the figure, the room temperature rolled sample has the highest ultimate tensile strength (UTS) of 550 MPa, but the lowest ductility with a total elongation of 3.2%. However, after recrystallization at both 700°C and 800°C, the ductility improved significantly to amounts of 13% and 19% in expense of little reduced tensile strength, respectively. The UTS level of recrystallized ODS copper at 800°C after room temperature rolling is superior to tensile strength of coarse grained pure copper (200 MPa) and also the recrystallized pure copper even after cryogenic rolling (~400 MPa) [4] and comparable with the precipitation strengthened CuCrZr (σ_y: 500 MPa) [3]. The high ductility in the recrystallized ODS copper at 800°C with a total elongation of 19% is attributed to the bimodal grain size distribution discussed previously in Ref. [4], consisting of ultrafine grains in combination to some micron sized grains as observed in the IPF map of Fig. 7 (b).

3.4. Deformation mechanism of ODS copper during rolling deformation

Investigation of the deformation mechanism was performed on the cold rolled ODS copper

deformed with 20% reduction by transmission electron microscope imaging. Based on the bright field TEM images in Fig. 9, one grain with a width of about 250 nm was selected to observe in four different g-vectors of $[31\bar{1}]$, $[200]$, $[\overline{11}1]$ and $[\bar{1}1\bar{1}]$ near to [011] zone axis as shown in each selected area diffraction pattern. According to Table 2, the visibility criteria ($|\vec{g}.\vec{b}|$values) was used for the evaluation of perfect dislocations and partial dislocations with the burgers vectors of $b_1 = \frac{a}{2}\langle 011\rangle$ and $b_2 = \frac{a}{6}\langle 211\rangle$, respectively. The detailed analysis of the four figures showed that the dislocation lines of three burgers vectors of $\frac{a}{2}[\bar{1}01]$, $\frac{a}{2}[0\bar{1}1]$, $\frac{a}{2}[1\bar{1}0]$ can be observed in these figures as shown by red arrows. In upper part of the images, a dislocation line between the grain boundary and an oxide particle with $\frac{a}{2}[1\bar{1}0]$ burgers vector is visible in all the figures except $g = [\overline{11}1]$. In the center part of the images, a zigzag dislocation line is located between some oxide particles with a length of ~100 nm which is invisible in the TEM image corresponding to $g = [200]$, possessing burgers vector of $\frac{a}{2}[0\bar{1}1]$. Furthermore, it was found different pieces of dislocations in the curved shape were in the lower part of the images which were realized to be a mixture of partial and perfect dislocations based on the visibility criteria. Except one perfect dislocation piece with $\frac{a}{2}[\bar{1}01]$ burgers vector shown by red arrows in other images, other segments can be distinguished more clearly in the image with g-vector of $[\bar{1}1\bar{1}]$. Moreover, a number of fine oxide particles can be distinguished around dislocation lines in this image. In other side, two finer pieces of dislocations with size of less than 20 nm (in $g\,(200)$ image) was found as the partial dislocations with $\frac{a}{6}[\bar{1}2\bar{1}]$

burgers vectors as shown by the yellow arrows.

Due to difficulty in observation of more partial dislocations in Fig. 9, the square area (in the $g(200)$ image), was evaluated in higher magnification in the same g-vectors in Fig. 10. In the $g(31\bar{1})$ and $g(200)$ (Fig. 10-a, b), a number of small blocks of stacking faults (SFs) were found with the length of 8 nm or less, marked by the red arrows as observed previously in the literature for the fcc Al [30]. In addition to the block-type stacking faults, in the two other images of $g(\bar{1}\bar{1}1)$ and $g(\bar{1}1\bar{1})$ (Fig. 10-c,d), numerous SF ribbons can be realized with a contrast of Moiré fringe patterns [31] as indicated by the yellow arrows. The shape of these fringe patterns is completely distinctive from the fringe contrast of oxide particles in spherical shape which has reported previously for oxide dispersion strengthened alloys [23]. These fringe patterns are the result of misfit dislocations in the interface of SF observed in appropriate diffraction condition, i.e, in g=<111> in our case. The formation of both types of ribbon and blocky SFs are indication in substantial existence of Shockley partial dislocations bearing burgers vector of $\frac{a}{6}\langle 211\rangle$. By measurement of more than seventy SF ribbons in the images, a wide range of 1.7-14 nm was obtained experimentally for the width of observed SFs while 90% of the SF ribbons have a size of less than 7nm.

4. Discussion

The results of grain structure evolution during cold rolling and recrystallization have been summarized in the schematic presentation of Fig. 11. As shown in this figure, during early

stages of cold rolling around 20% thickness reduction, the primary submicron sized grains with α-fiber texture (Fig. 11(a)) refine to fine grain size of ~0.25 μm with increasing dislocation density and intensity of brass texture grains enhances in expense of other orientations (Fig. 11(b)). Progress of rolling up to 60% thickness reduction lead to gradual promotion of the grain size in simultaneous to reorientation of different texture grains to higher fraction of brass texture grains (Fig. 11(c)). The rate of change in microstructure and texture development from 60% to 80% thickness reduction amplify wonderfully based on the results presented in Fig. 5 and leads to formation of a heavily deformed single-crystal brass texture grain inside the whole 80% rolled sample as the matrix including many ultrafine subgrains developed by high density low angle dislocation boundaries (Fig. 11(d)). During annealing of 80% rolled sample, again ultrafine grains with an average grain size of 1 μm formed inside the microstructure (Fig. 11(e)). The cold rolled microstructure showed a retardation in nucleation of new recrystallized grains and according to the microhardness results (Fig. 6), it shifts to high recrystallization regime of around 700ºC/30 min. This temperature is far from the typical recrystallization temperature reported for cold rolled pure copper to be around 200 ºC for a few minutes [4,5]. The large difference between recrystallization temperature of ODS copper and pure copper can be interpreted with respect to distribution of fine nanosized oxide particles and obtained grain structure. Fine distribution of oxide particles are effective barriers against recrystallization based on the Zenner pinning force per unit area (P) in the following relation [32]:

$$P = 3f\gamma/2r \quad (4\text{-}1)$$

where, f and r are the volume fraction (~0.0075) and radius of oxide particles (~5 nm) and γ is the grain boundaries energy (~1 J/m^2). So, there is a pinning energy of ~1.8 MJ by oxide particles. Furthermore, formation of large millimeter-sized grain in 80% cold rolled ODS copper reduced the fraction of HABs significantly. As the HABs are favored sites for nucleation during recrystallization [28,33], the recrystallization retards to much higher temperatures.

According to Fig. 9, existence of two types of perfect dislocations with $\frac{a}{2}[1\bar{1}0]$ burgers vector and Shockley partial dislocations of $\frac{a}{6}[\bar{1}2\bar{1}]$ burgers vectors proved in 20% reduction rolled ODS copper by TEM imaging. Based on the observations, the perfect dislocations had a higher length of typical 100 nm in a ragged arrangement caused through pinning of dislocation lines by fine oxide particles. The repulsive interaction of dislocations by oxide particles has been established before by Scattergood and Bacon [34] based on the Orowan mechanism and results in strengthening effect especially at high temperatures [1]. Such a strong pinning of perfect dislocation lines can be observed in 80% rolled ODS copper with a higher dislocation density in TEM image of Fig. 12(a), which demonstrates looping of dislocations around fine oxide particles in different locations indicated by arrows. Therefore, a pinned perfect dislocation with $\frac{a}{2}[10\bar{1}]$ burgers vector dissociates into two finer partial dislocations of $\frac{a}{6}[11\bar{2}]$ and $\frac{a}{6}[2\bar{1}1]$ burgers vectors by the following reaction leaving a SF in (111) plane according to Fig. 12(b):

$$\overrightarrow{b_1} \rightarrow \overrightarrow{b_2} + \overrightarrow{b_3} \quad (4\text{-}2)$$

$$\frac{a}{2}[10\bar{1}] \rightarrow \frac{a}{6}[11\bar{2}] + \frac{a}{6}[2\bar{1}1] \quad (4\text{-}3)$$

Entity of a high number of nanosized SFs in the microstructure (Fig. 10) suggests extensive dissociation of perfect dislocations into a high density of Shockley partial dislocations during deformation of ODS copper.

Up to now, two main factors have been proposed for Brass texture evolution in copper alloys: twinning [15] and shear bands [5,16]. In this study on ODS copper, the fraction of nanotwins is about 6% limited to very small high strain areas without observation of shear bands. Recently, Gu et al. [18] proposed a different deformation mechanism using simulation approach in ultrafine-grained copper associated with the activation of partial $\{110\}\langle 11\bar{2}\rangle$ slip in addition to usual $\{111\}\langle 110\rangle$ slip. In our theory in accordance with Fig 12(c), the primary submicrometer grains with wide orientations of Goss to Brass deform during room temperature rolling by mechanism of partial slip of $\frac{a}{6}\langle 211\rangle$ burgers dislocations in a random approach in four $\{111\}$ slip planes of fcc copper structure. The glide of partial dislocations in either two slip planes of (111) and $(11\bar{1})$ or $(1\bar{1}1)$ and $(1\bar{1}\bar{1})$ in each grain gives an outcome deformation in $\{110\}$ plane with $\langle 211\rangle$ direction, i.e. “Brass orientation”. In parallel, moving of some partial dislocations in the neighboring planes results in formation of nanoscale twins. Hence, by increasing the rolling reduction or deformation strain and as a result higher activity of partial dislocations, the grains tend to rotate into the stronger Brass orientation.

Based on the grain structure evolution in Fig. 4 and 5(a), while the grain structure is still in micrometer scale until 60% thickness reduction, higher deformation up to 80% reduction leads to coarsening of individual Brass-oriented grains and final formation of single grain Brass-oriented deformed structure.

Conclusions

In this study, the grain structure, texture evolution and tensile properties of ODS copper after room temperature cold rolling and subsequent recrystallization was investigated and the below conclusions were obtained:

1. The fine grain structure coarsened during room temperature rolling in simultaneous to development of Brass texture especially after 60% reduction and finally, a single millimeter sized brass texture deformed grain was evolved in 80% reduction room temperature rolled ODS copper.
2. Recrystallization of ODS copper retarded to the high temperature of ~700°C mainly due to Zener pinning force of fine oxide particles. A fine-grained microstructure with the new textures of α and β-fiber including Goss, Brass, S and copper components were developed in the recrystallized condition.
3. Pinning of perfect dislocations with burgers vector of $\frac{a}{2}\langle 101\rangle$ happened by distribution of fine oxide particles and deformation mechanism was controlled via high activity of partial dislocations with burgers vector of $\frac{a}{6}\langle 211\rangle$ in a random approach.
4. Tensile properties of recrystallized ODS copper at 800°C for 30 min showed a high UTS of 491 MPa with a good ductility of 19% at ambient temperature. This combined high tensile strength-ductility was attributed to bimodal grain size distribution including ultrafine grained together with micron sized grained structure.

Acknowledgements

The first author gratefully acknowledges Prof. Hashimoto and Prof. Zinkle for their valuable discussions in this study. This work was supported by Grant-in-Aid for Scientific

Research(A), 16H02443, Japan Society for the Promotion of Science (JSPS).

References

1. S. Ukai, Oxide Dispersion Strengthened Steels, in: R.M.J. Konings (Eds.), Comprehensive Nuclear Materials, Vol. 4, Elsevier Ltd., 2012, pp. 241–271.
2. J. Knaster, A. Moeslang and T. Muroga, Materials research for fusion, Nat. Phys., Vol. 12, 2016, 424-434.
3. M. Li, S. J. Zinkle, Physical and Mechanical Properties of Copper and Copper Alloys, in: R.M.J. Konings (Eds.), Comprehensive Nuclear Materials, Vol. 4, Elsevier Ltd., 2012, 667-690.
4. Yinmin Wang, Mingwei Chen, Fenghua Zhou & En Ma, High tensile ductility in a nanostructured metal, Nat., Vol. 419, 2002, 912-915.
5. L. Lapeire, J. Sidor, P. Verleysen, K. Verbeken, I. De Graeve, H. Terryn, L.A.I. Kestens , Texture comparison between room temperature rolled and cryogenically rolled pure copper, Acta Mater. 95, 2015, 224–235.
6. C.F. Gu, M. Hoffman, L.S. Toth, Y.D. Zhang, Grain size dependent texture evolution in severely rolled pure copper, Mater. Charact. 101, 2015, 180–188.
7. Y. Sutou, T. Omori a, K. Yamauchi a, N. Ono b, R. Kainuma c, K. Ishida, Effect of grain size and texture on pseudoelasticity in Cu–Al–Mn-based shape memory wire, Acta Mater. 53, 2005, 4121–4133.
8. L. Llanesi, A. D. Rollett, C. Laird and J. L. Bassani, Effect of grain size and annealing texture on the cyclic response and the substructure evolution of polycrystalline copper, Acta Metall Mater 41, 1993, 2667-2679.
9. F. J. Humphreys, M. Hatherly, Recrystallization and related annealing phenomena, Second Edition, Elsevier, 2004.
10. T. Konkova, S. Mironov, A. Korznikov, S.L. Semiatin, Microstructural response of pure copper to cryogenic rolling, Acta Mater. 58, 2010, 5262–5273.
11. Y. Jiang, J. T. Wang, Y. Wang, J. Yin, Investigation on Grain Size Effect of Rolling Texture in Copper , Mater. Sci. forum, 2016, 850, 857-863.
12. J.X. Zhang, M. Ma, W.C. Liu, Effect of initial grain size on the recrystallization and recrystallization texture of cold-rolled AA 5182 aluminum alloy, Mater. Sci. Eng. A 690, 2017, 233–243.
13. P. P. Bhattacharjee, M. Joshi, V.P. Chaudhary, M. Zaid, The effect of starting grain size on the evolution of microstructure and texture in nickel during processing by cross-rolling, Mater Charact. 76, 2013, 21–27.
14. A. Salinas-rodriguez, Grain size effects on the texture evolution of α-Zr, Acta Metall, Mater. 4, 1995, pp. 485-498.
15. T. Leffers, R. K. Ray, The brass-type texture and its deviation from the copper-type texture, Prog. Mater. Sci. 54, 2009, 351–396.
16. E. El-danaf, S. R. Kalidindi, R. D. Doherty and C. Necker, Deformation Texture Transition in Brass: Critical Role of Micro-Scale Shear Bands, Acta Mater. 48 (2000) 2665–2673.
17. W. Skrotzki, A. Eschke, B. Jo´ni, T. Unga´r, L.S. To´th, Yu. Ivanisenko, L. Kurmanaeva, New experimental insight into the mechanisms of nanoplasticity, Acta Mater. 61, 2013, 7271–7284.
18. C.F. Gu, L.S. Toth, Y.D. Zhang and M. Hoffman, Unexpected brass-type texture in rolling of ultrafine-grained

copper, Scri Mater 92, 2014, 51–54.
19. N. Hansen and T. Leffers, Microstructures, textures and mechanical properties after large strain, Revue Phys. Appl. 23, 1988, 519-531.
20. S. M. S. Aghamiri, N. Oono, S. Ukai, R. Kasada, H. Noto, Y. Hishinuma, T. Muroga, Microstructure and mechanical properties of mechanically alloyed ODS copper alloy for fusion material application, Nucl. Mater. Ene., in Press.
21. D. B. Williams, C. Barry Carter, Transmission Electron Microscopy, A textbook for materials science, Springer, 2nd edition, 2009.
22. K. N. Zhu, A. Godfrey, N. Hansen, X. D. Zhang, Microstructure and mechanical strength of near- and sub-micrometre grain size copper prepared by spark plasma sintering, Mater. & Des. 117 (2017) 95-103.
23. P. Dou, A. Kimura, T. Okuda, M. Inoue, S. Ukai, S. Ohnuki, T. Fujisawa, F. Abe, Polymorphic and coherency transition of Y–Al complex oxide particles with extrusion temperature in an Al-alloyed high-Cr oxide dispersion strengthened ferritic steel, Acta Mater. 59 (2011) 992–1002.
24. Y.S. Li, N.R. Tao, K. Lu, Microstructural evolution and nanostructure formation in copper during dynamic plastic deformation at cryogenic temperatures, Acta Mater. 56 (2008) 230–241.
25. D. A. Hughes and N. Hansen, Microstructure and strength of nickel at large strains, Acta Mater. 48, 2000, 2985–3004.
26. Q. Liu, X. Huang, D.J. Lloyd, N. Hansen, Microstructure and strength of commercial purity aluminium (AA 1200) cold-rolled to large strains, Acta Mater. 50, 2002, 3789–3802.
27. N. Hansen, Cold deformation microstructures, Mater. Sci. Tech.6,1990, 1039-1047.
28. Fengxiang Lin, Recrystallization of deformed copper - kinetics and microstructural evolution, Phd thesis, Technical University of Denmark, March 2013.
29. T. Konkova, S. Mironov, A. Korznikov, M.M. Myshlyaev, S.L. Semiatin, Annealing behavior of cryogenically-rolled copper, Mater. Sci. Eng. A 585 (2013) 178–189.
30. X. Z. Liao, F. Zhou, E. J. Lavernia, S. G. Srinivasan, M. I. Baskes, D. W. He, and Y. T. Zhu, Deformation mechanism in nanocrystalline Al: Partial dislocation slip, Appl. Phys. Lett. 83, 632, 2003.
31. D. Hull and D. J. Bacon, Introduction to Dislocations, Fifth Edition, Elsevier, 2011.
32. D. A. Porter, K. E. Easterling and M. Y. Sherif, Phase transformations in metals and alloys, Third Edition, CRC press, 2009.
33. H. W. F. Hellerp, C. A. Verbraaks and b. H. Kolster, Recrystallization at grain boundaries in deformed copper bicrystals, Acta Mater. 32, 1984, 1391-1406.
34. R. O. Scattergood and D. J. Bacon, The Orowan mechanism in anisotropic crystals, Phil. Mag. A 31 (1975) 179-198.

List of Figures

Fig. 1

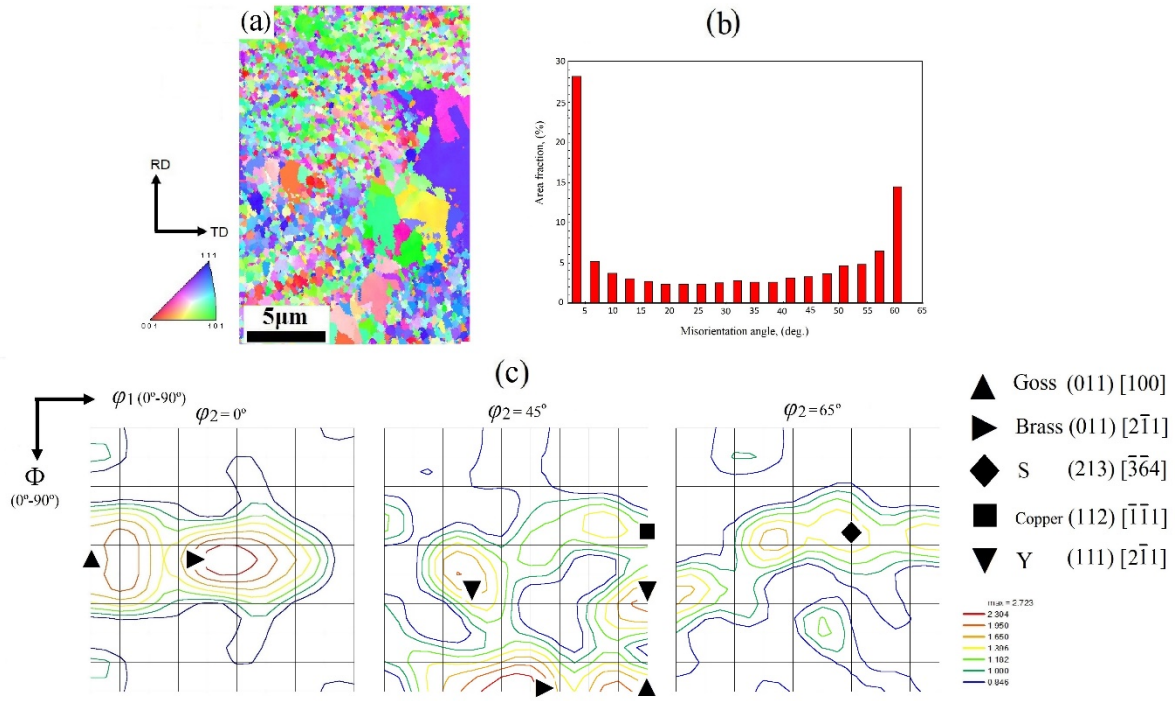
(a)
RD
TD
5μm
(b)
Area fraction, (%)
Misorientation angle, (deg.)
(c)
φ1 (0°-90°)
Φ
(0°-90°)
φ2 = 0°
φ2 = 45°
φ2 = 65°
Goss (011) [100]
Brass (011) [2$\bar{1}$1]
S (213) [$\bar{3}\bar{6}$4]
Copper (112) [$\bar{1}\bar{1}$1]
Y (111) [2$\bar{1}$1]

Fig. 2

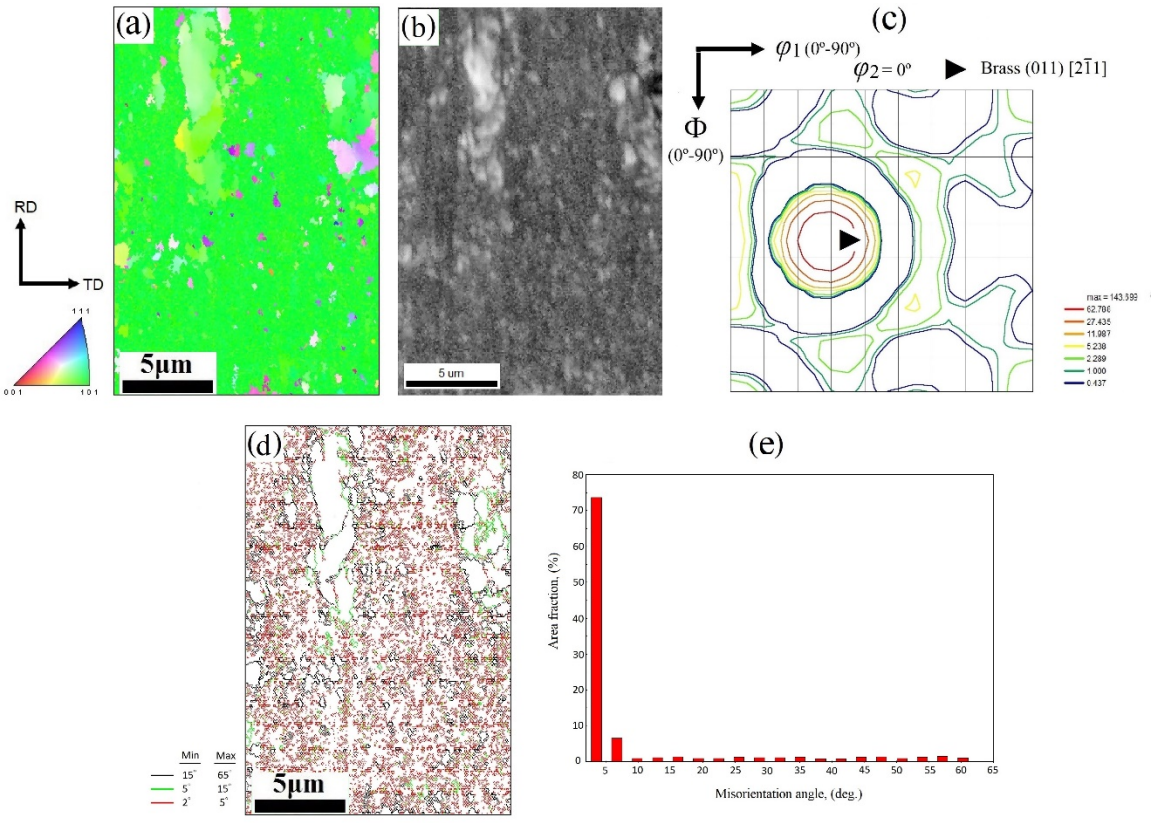
(a)
RD
TD
5μm
(b)
5 um
(c)
φ1 (0°-90°)
φ2 = 0°
Brass (011) [2$\bar{1}$1]
Φ
(0°-90°)
(d)
Min
Max
15°
65°
5°
15°
2°
5°
5μm
(e)
Area fraction, (%)
Misorientation angle, (deg.)

Fig. 3

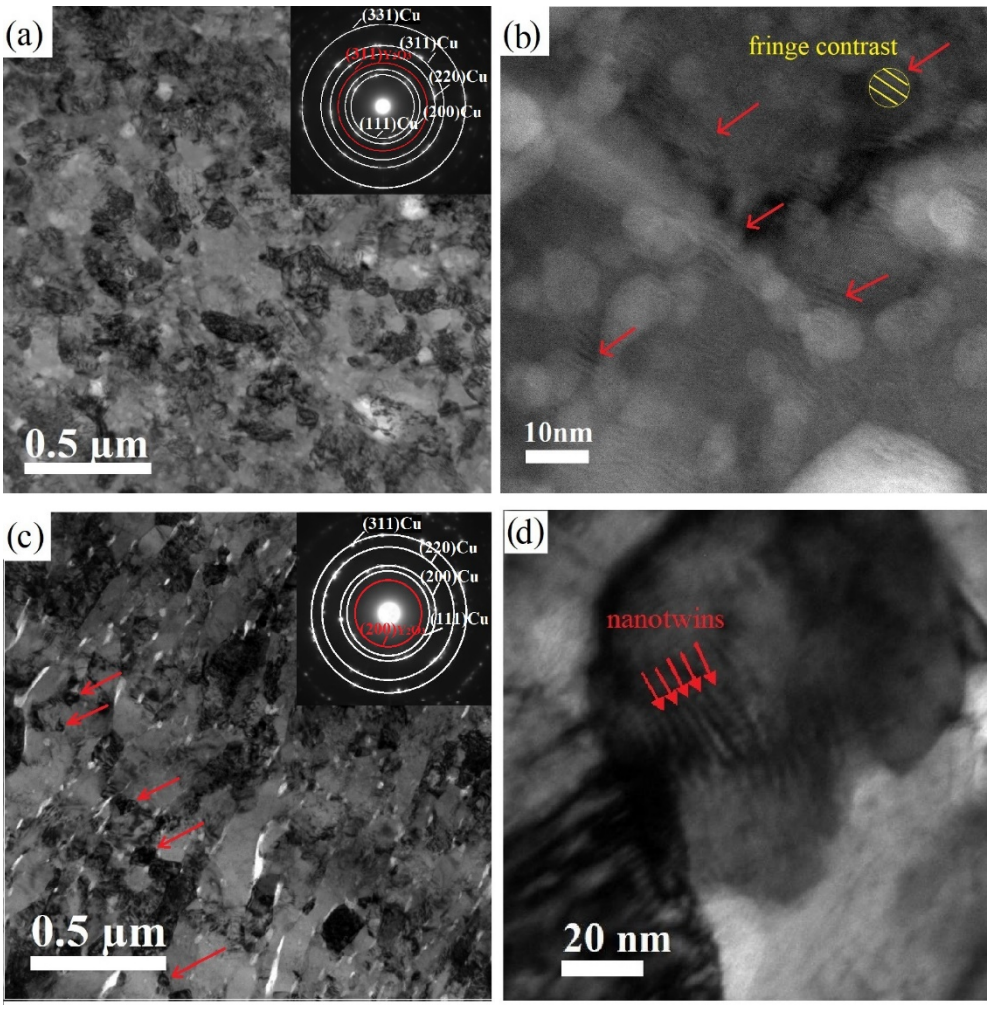
(a)
(331)Cu
(311)Cu
(220)Cu
(200)Cu
(111)Cu
0.5 μm
(b)
fringe contrast
10nm
(c)
(311)Cu
(220)Cu
(200)Cu
(111)Cu
0.5 μm
(d)
nanotwins
20 nm

Fig. 4

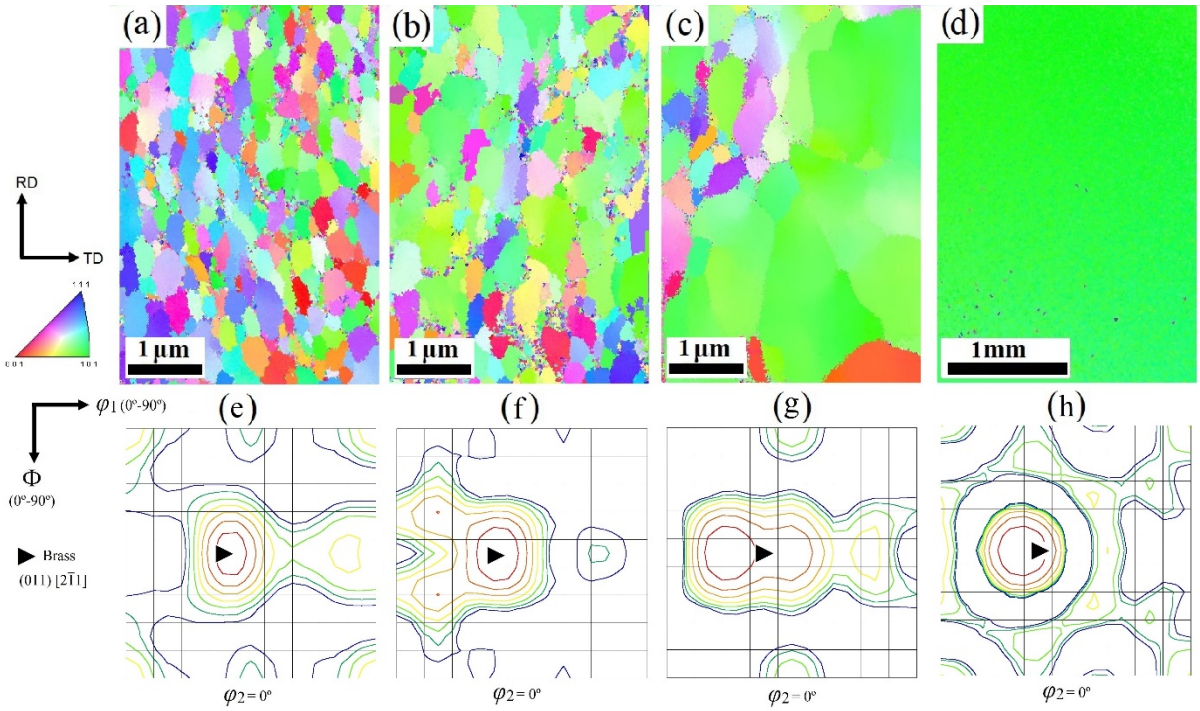
(a)
(b)
(c)
(d)
RD
TD
1 µm
1 µm
1 µm
1mm
φ1 (0°-90°)
Φ
(0°-90°)
Brass
(011) [2$\bar{1}$1]
(e)
(f)
(g)
(h)
φ2 = 0°
φ2 = 0°
φ2 = 0°
φ2 = 0°

Fig. 5

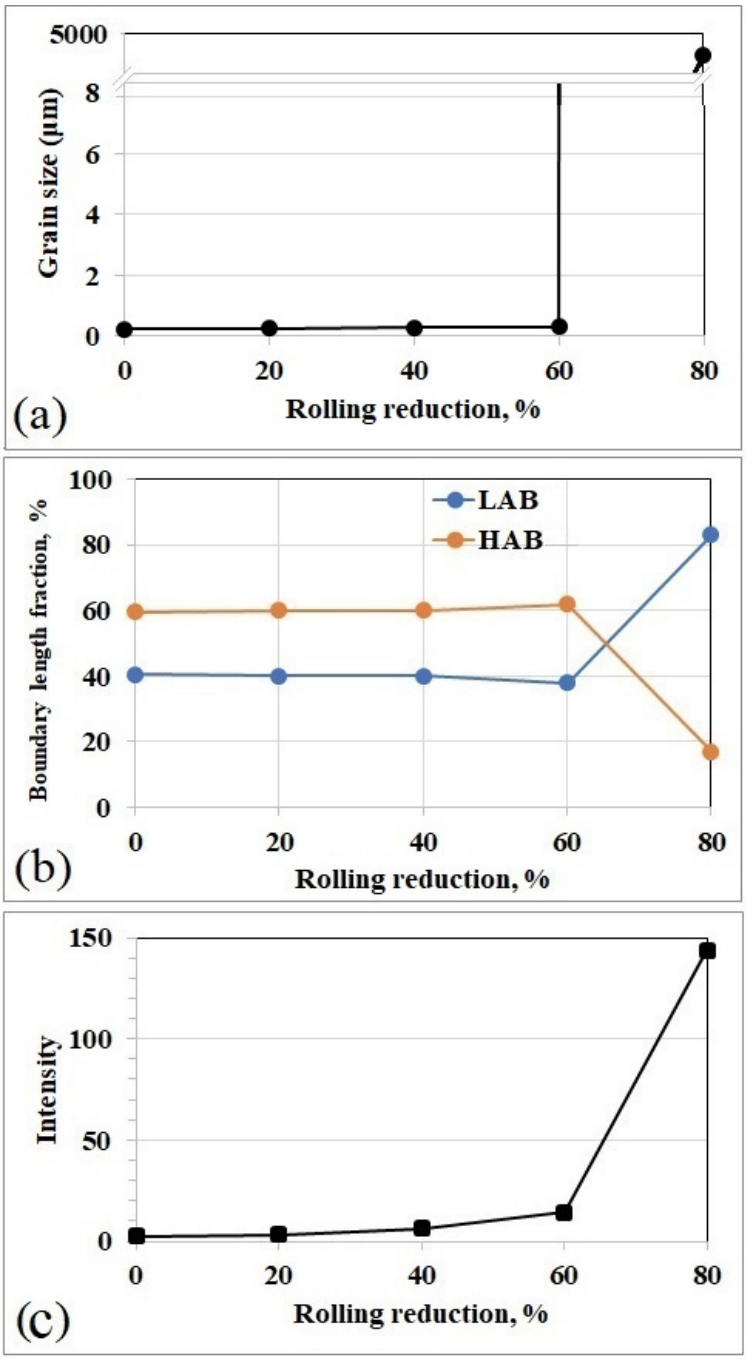
5000
8
6
4
2
0
Grain size (μm)
0
20
40
60
80
Rolling reduction, %
(a)
100
80
60
40
20
0
Boundary length fraction, %
LAB
HAB
0
20
40
60
80
Rolling reduction, %
(b)
150
100
50
0
Intensity
0
20
40
60
80
Rolling reduction, %
(c)

Fig. 6

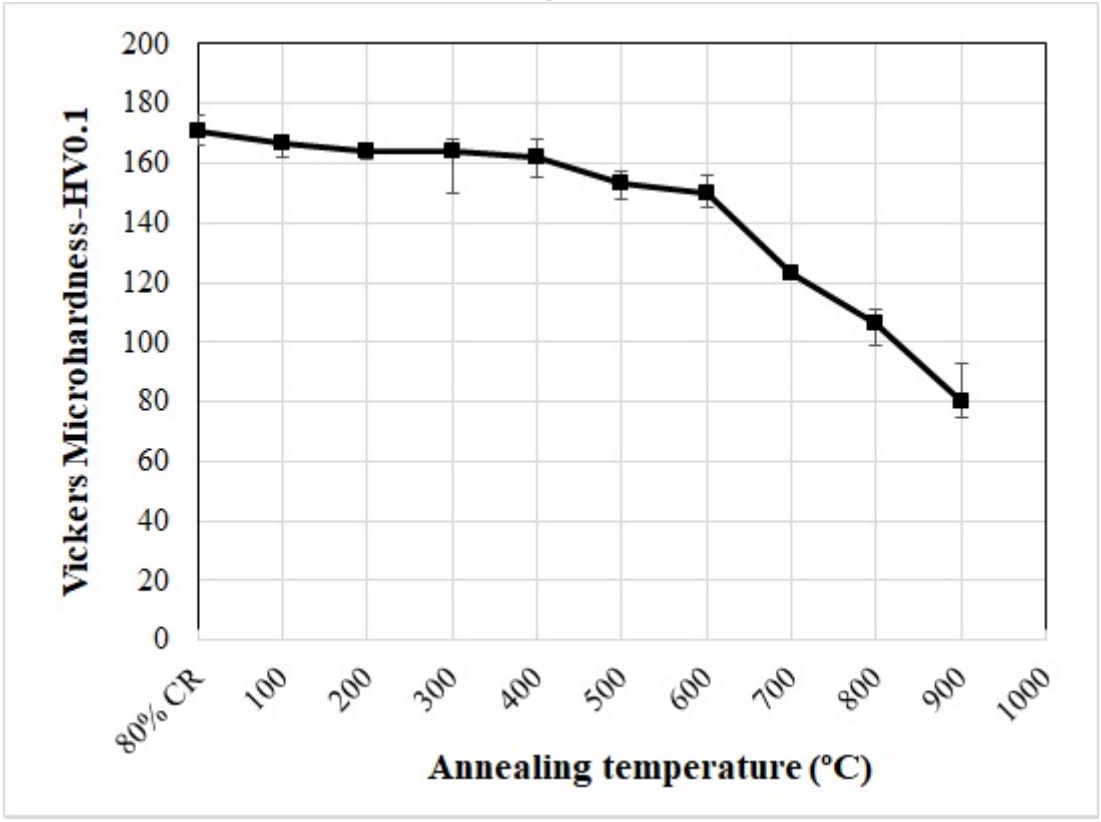
Vickers Microhardness-HV0.1
200
180
160
140
120
100
80
60
40
20
0
80% CR
100
200
300
400
500
600
700
800
900
1000
Annealing temperature (°C)

Fig. 7

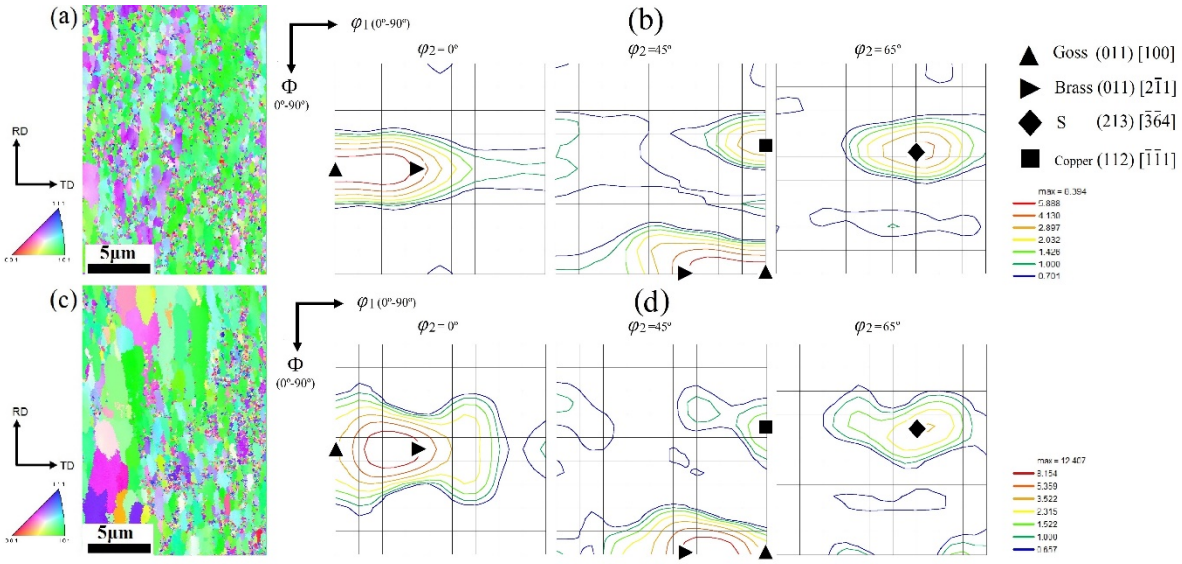
(a)
RD
TD
5μm
(b)
(c)
(d)
φ1 (0°-90°)
Φ
(0°-90°)
φ2 = 0°
φ2=45°
φ2=65°
Goss (011) [100]
Brass (011) [2$\bar{1}$1]
S (213) [$\bar{3}\bar{6}$4]
Copper (112) [$\bar{1}\bar{1}$1]

Fig. 8

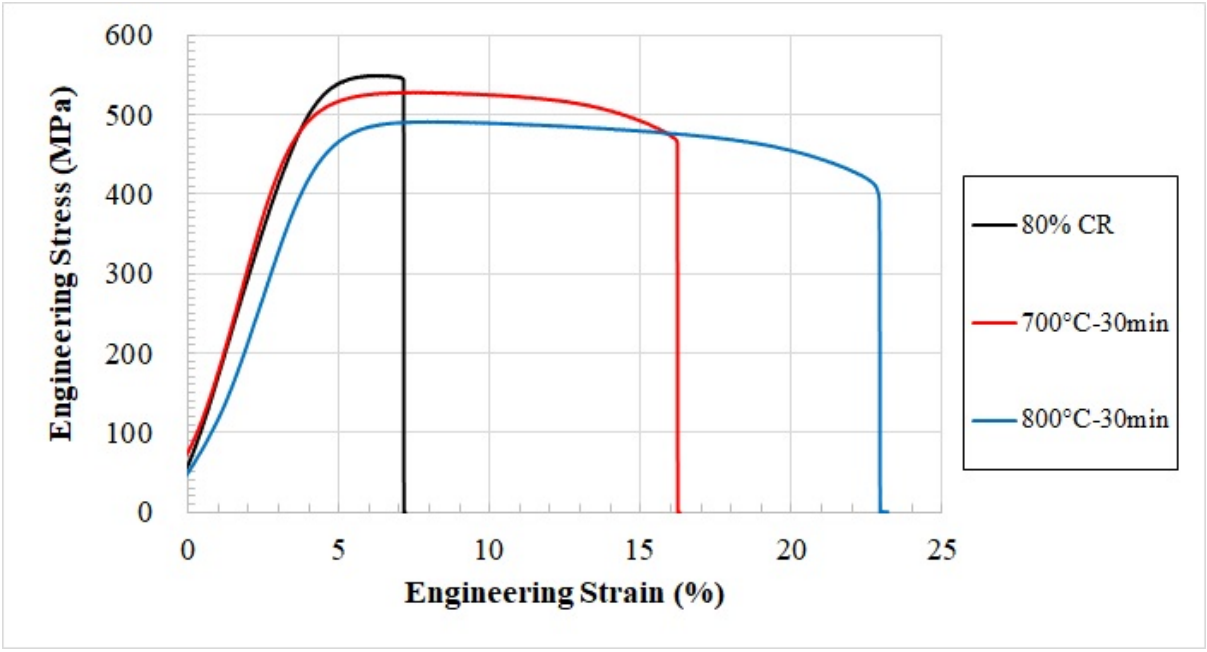
Engineering Stress (MPa)
600
500
400
300
200
100
0
0
5
10
15
20
25
Engineering Strain (%)
80% CR
700°C-30min
800°C-30min

Fig. 9

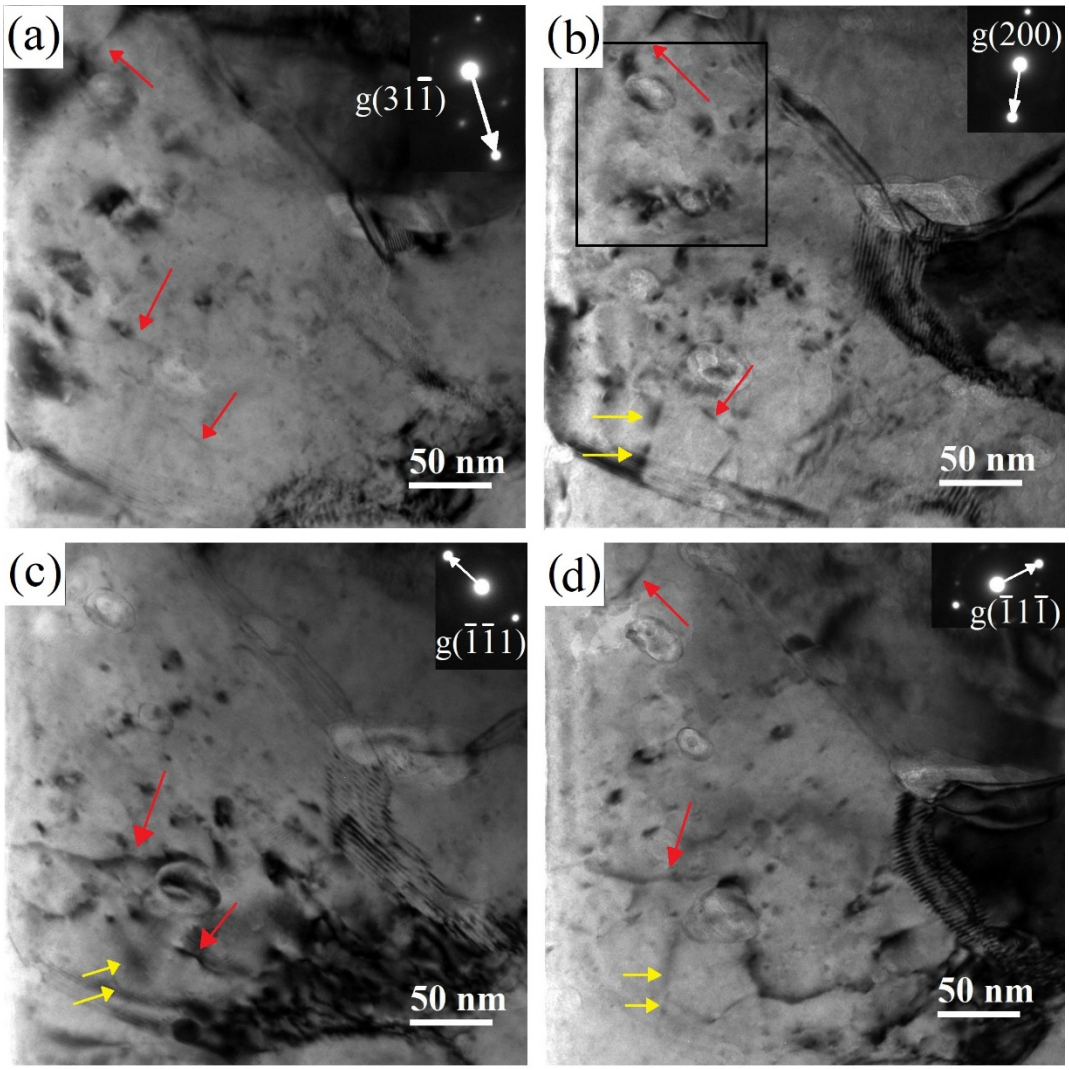
(a)
g(31$\bar{1}$)
50 nm
(b)
g(200)
50 nm
(c)
g($\bar{1}\bar{1}$1)
50 nm
(d)
g($\bar{1}$1$\bar{1}$)
50 nm

Fig. 10

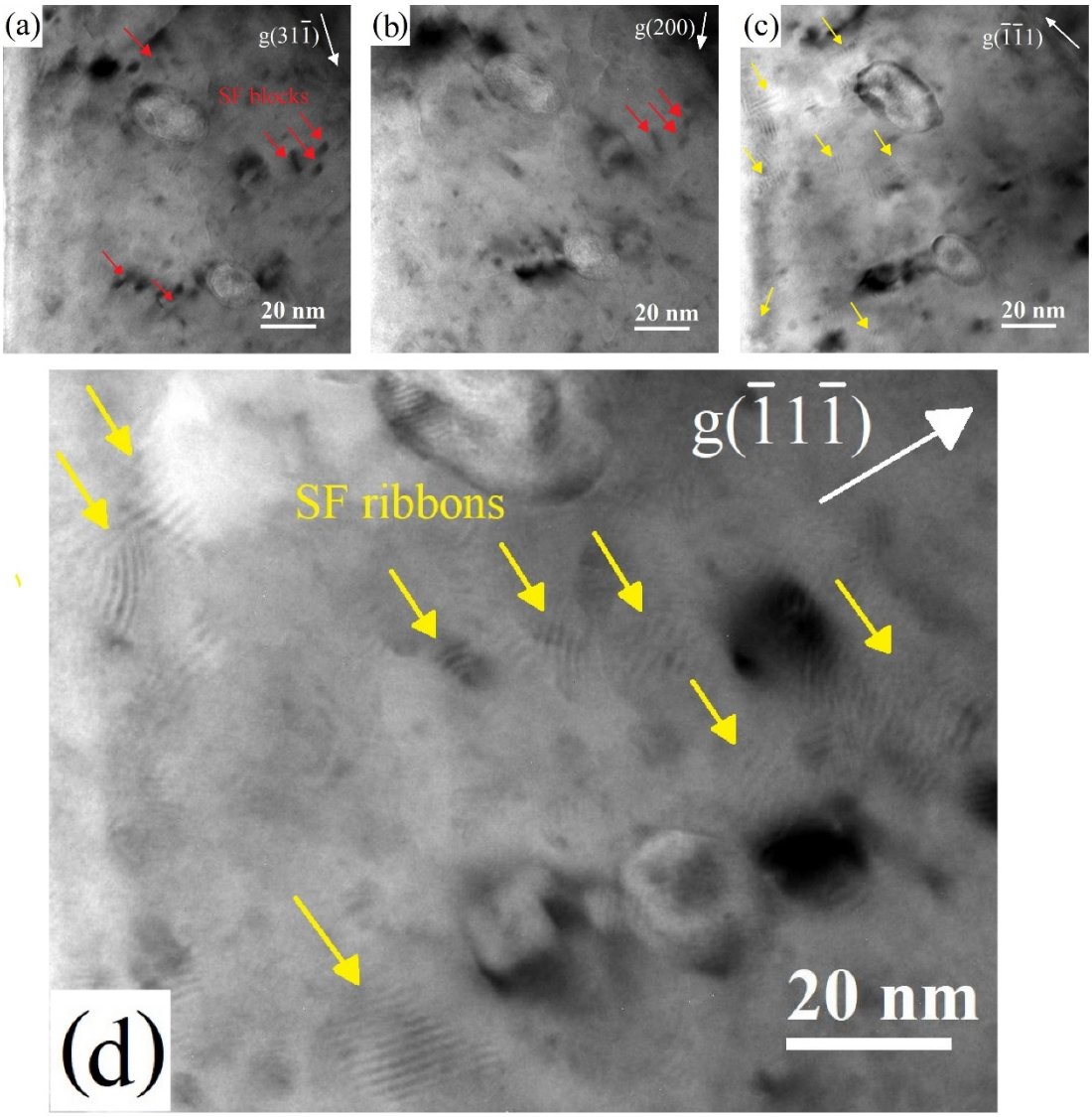
(a)
g(31$\bar{1}$)
SF blocks
20 nm
(b)
g(200)
20 nm
(c)
g($\bar{1}\bar{1}$1)
20 nm
g($\bar{1}$1$\bar{1}$)
SF ribbons
20 nm
(d)

Fig. 11

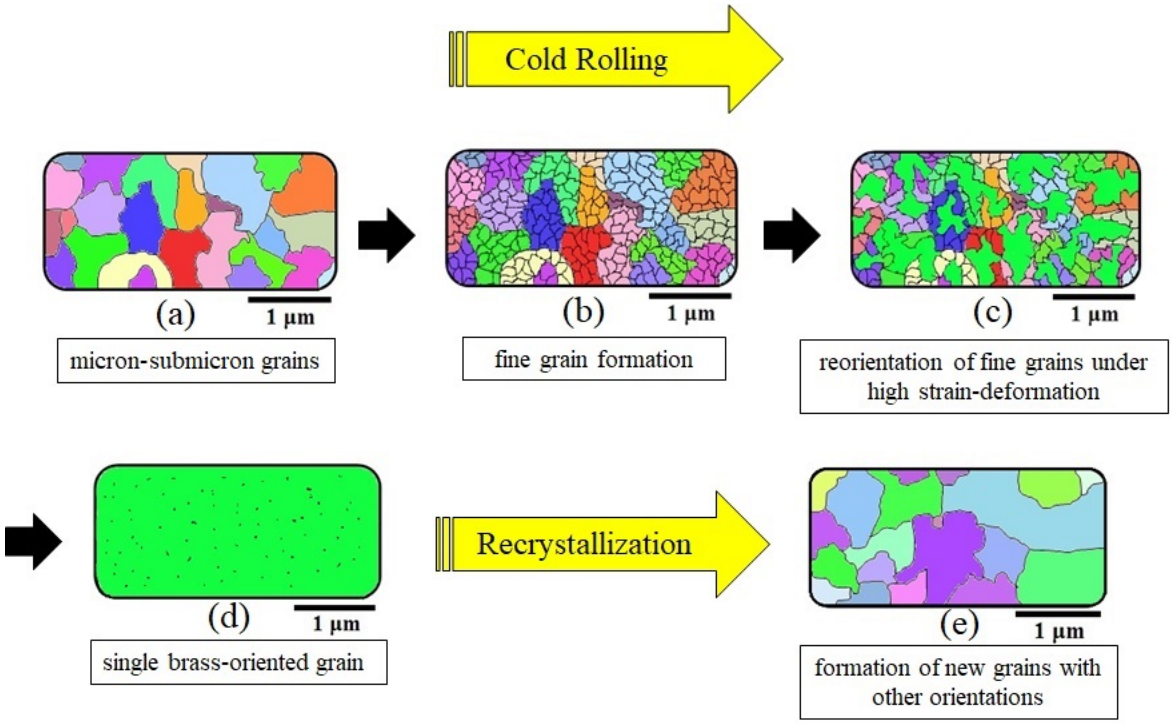
Cold Rolling
(a)
1 μm
micron-submicron grains
(b)
1 μm
fine grain formation
(c)
1 μm
reorientation of fine grains under high strain-deformation
(d)
1 μm
single brass-oriented grain
Recrystallization
(e)
1 μm
formation of new grains with other orientations

Fig. 12

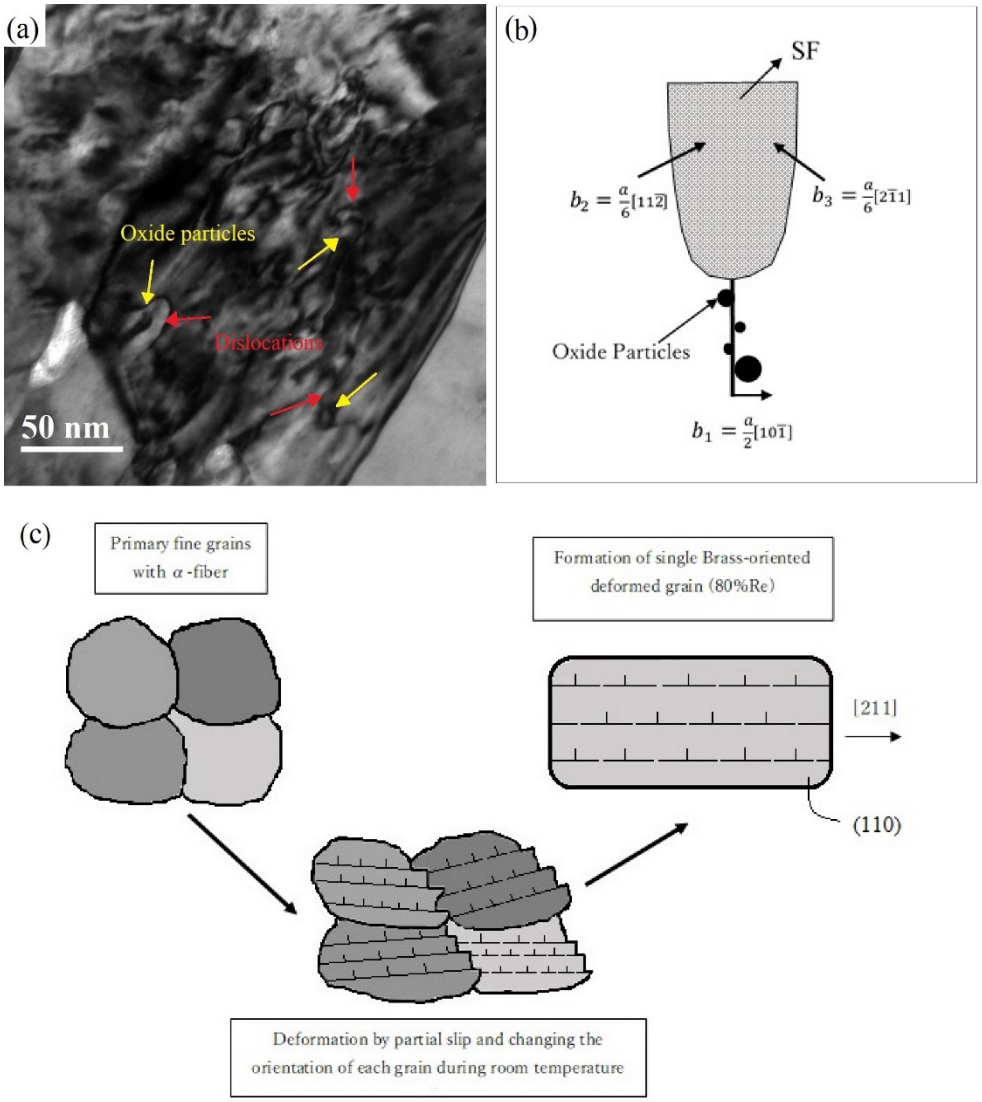
(a)
Oxide particles
Dislocations
50 nm
(b)
SF
$b_2 = \frac{a}{6}[11\bar{2}]$
$b_3 = \frac{a}{6}[2\bar{1}1]$
Oxide Particles
$b_1 = \frac{a}{2}[10\bar{1}]$
(c)
Primary fine grains with α-fiber
Formation of single Brass-oriented deformed grain (80%Re)
[211]
(110)
Deformation by partial slip and changing the orientation of each grain during room temperature

List of Tables

Table 1. Values of mechanical properties of 80% reduction room temperature rolled and subsequent recrystallized ODS copper at 700°C and 800°C for 30 min.

Table 1

Sample	$\sigma_{0.2}$	σ_u	el_u (%)	el_t (%)
Roll. 80% Re.	480	550	2.3	3.2
Rec. 700°C/30	460	528	4.2	13
Rec. 800°C/30	422	491	3	19

Table 2. $|\vec{g}.\vec{b}|$ value for different g-vectors near to [011] zone axis

Table 2

$\vec{g}$ \ $\vec{b}$	1/6[11-2]	1/6[-12-1]	1/6[2-1-1]	1/2[-101]	1/2[0-11]	1/2[1-10]
(31-1)	1	0	1	-2	-1	1
(200)	1/3	-1/3	2/3	-1	0	1
(-1-11)	-2/3	-1/3	-1/3	1	1	0
(-11-1)	1/3	2/3	-1/3	0	-1	-1